Flatness-based Motion Planning and Model Predictive Control of Industrial Cranes

Hoa Bui Thi Khanh
Faculty of Electrical Engineering, Hanoi University of Industry, Vietnam | Hanoi University of Science and Technology, Vietnam
hoabtk@haui.edu.vn

Mai Hoang Thi
Department of Automation, SEEE, Hanoi University of Science and Technology, Vietnam
Mai.HT232216M@sis.hust.edu.vn

Luu Thi Hue
Department of Electrical Engineering, Electric Power University, Vietnam
huelt@epu.edu.vn (corresponding author)

Tung Lam Nguyen
Department of Automation, SEEE, Hanoi University of Science and Technology, Vietnam
lam.nguyentung@hust.edu.vn

Danh Huy Nguyen
Department of automation, SEEE, Hanoi University of Science and Technology, Vietnam
huy.nguyendanh@hust.edu.vn

Received: 28 April 2024 | Revised: 15 May 2024 | Accepted: 25 May 2024

 DOI: https://doi.org/10.48084/etasr.7662

ABSTRACT

This study develops a new controller for an industrial crane system in a three-dimensional space. First, the dynamic model of the industrial crane system with two subsystems, the tower crane and the overhead crane is presented. A bidirectional mapping is established between the system's input and output, allowing for efficient trajectory generation. Additionally, the design process explicitly considers the system's kinematic constraints, ensuring safe and feasible motions. This designed trajectory serves as an input for Model Predictive Control (MPC). The MPC is designed with the dual objectives of trajectory tracking and payload anti-swing. Finally, simulations are conducted and the results are compared with those of other control strategies under different cases to demonstrate the effectiveness of the proposed method.

Keywords-tower crane; gantry crane; flatness; three-dimensional tower crane; model prediction controller

I. INTRODUCTION

Cranes are designed and built into all sizes for different applications. The load transportation requires the combination of the cooperative motions of the trolley and the lifting and lowering motion of the payload. These actions must simultaneously be performed to reduce traveling time. However, moving at a high speed increases the payload swing angles, which can be dangerous to people and surrounding structures. While moving at low speed, although the swing angle of the payload is reduced, the transport efficiency of the three-Dimensional Overhead Crane (3DOC) system is also reduced. Therefore, the problem of designing an optimal time-based motion trajectory for the three-Dimensional Tower Crane (3DTC) system is obvious, ensuring both small payload swing and system performance. The problem of reducing load vibration during the positioning process of a 3DOC system is presented in [1, 2]. In addition, a stable time optimization technique with input shaping is used to control vibration [3]. The online synthetic trajectory design method is proposed in [4]. The proposed trajectory ensures the moving position of the jib and trolley and ensures the swing angle with the damping component. A real-time trajectory design method for a tower crane system with variable lengths to raise/lower loads is presented in [5]. The time-optimal anti-swing controller is suggested in [6] deploying a low-pass filter to achieve minimal swing angle and a smooth velocity trajectory to avoid jerk. In [7], a time-optimal motion and an energy consumption controller for crane systems are developed, in which the constraints of the actuator on velocity and acceleration are considered. Authors in [8, 9] introduce an optimal trajectory solution based on a time polynomial for tower cranes, which

aims to minimize transportation time while satisfying various constraints. In [10], an optimal controller for reducing transition time and path error is developed for a five Degree of Freedom (5DOF) tower crane system to compute the transition trajectory between two reference points. The mentioned above real-time optimal algorithms employ a significant computational burden to the controllers, which makes practical implementation difficult. To solve this problem, the flatness-based theory is utilized to construct the motion planning for the 3DTC system. At this point, the problem becomes motion planning for the payload satisfying the constraints. The control signal and state variables can be expressed as functions of the payload position and its level derivatives. As in [11], a backstepping controller combined with trajectory planning is proposed to prevent an antisway problem in the overhead crane system under wind disturbances. The desired trajectory is acquired by solving the optimal parameter problem of flat output based on the time-flatness of the underactuated crane system and the tracking controller [12, 13].

In addition to developing a time-optimal trajectory that satisfies the constraints to improve the performance of the crane system, the control issue is also of equal concern. Adaptive control for a double-pendulum overhead crane with an uncertain model and external disturbances is presented in [14], guaranteeing the position error of the trolley within a permissible bound, and quickly converging to zero. The construction of a controller that considers variable cable length to improve robustness, accurate tracking, and more effective anti-vibration of payloads is suggested in [15, 16]. Adaptive fuzzy controllers [17, 18] overcome the uncertainty model and compensate for external disturbances in the tower crane system. The controller ensures reduced vibration of the payload when transported to the desired position. The recommended nonlinear adaptive backstepping controller in [19] eliminates the pendulum swing and positioning for the crane. An adaptive payload lifting/lowering tracking controller for double-pendulum cranes, which accurately tracks and suppresses the oscillation of the double-pendulum while estimating the unknown parameters of gravity, is presented in [20]. An adaptive input shaper for payload swing control in a tower crane with uncertain parameters and obstacle avoidance is introduced in [21]. The shaper parameters are updated based on the current parameters of the crane. The crane system is moved by the drive system, which can only respond within a limit. All the above controllers are designed without considering input constraints or the conditions of the state variables. The Model Predictive Controller (MPC) takes into account the system constraints when designing the controller. In [22], an MPC approach is built upon the designed system model, which minimizes an objective function that integrates both energy cost and swing angle. In [23], an MPC controller is implemented for the internal control loop of a tower crane. This approach generates references that achieve both accurate tracking of the desired position and efficient damping of payload oscillations. In [24], a distributed MPC scheme for 3DTC that ensures asymptotic stability by utilizing three independent MPC controllers, each designed to be locally stabilizing, is introduced.

Based on the flatness-based theory, this paper presents a motion planning approach for the payload that satisfies the conditions of the 3DTC system. This designed trajectory serves as an input for MPC, with input constraints and system state variables to improve the ability to better control the payload. By exploiting the system's flatness property, a bidirectional mapping is established between the system's input and output, allowing for efficient trajectory generation. Additionally, the design process explicitly considers the system's kinematic constraints, ensuring safe and feasible motions. The MPC strategy for the dual objectives of trajectory tracking and payload anti-swing control is proposed. The MPC controller guarantees the stability of the closed-loop system.

II. MODEL OF INDUSTRIAL CRANES

The structures of the 3DOC and 3DTC can be seen in Figure 1. The 3DTC consists of three main parts: a supporting column and rotating rod with an equivalent moment of inertia J_0, the car with mass M_t, and the load with mass m. To bring the load to the desired position, the rotary bar is rotated at an angle γ and the trolley is moved to the desired position. The coordinates of the load will be determined indirectly through the vector $\mathbf{q}=[\gamma,x,l,\phi,\theta]^T$, where x is the position of the cart in the x-axis, l is the length of the cable, ϕ is the angle of the rotation of the load relative to the x-axis, and θ is the angle of the rotation of the load relative to the y-axis. The tower crane is a MIMO system with three control inputs: the force acting on the trolley cap F_x, the force acting on the rope cap F_l, and the rotating rod τ_γ. Then, the control signal vector is defined as $U=[\tau_\gamma,f_x,f_l,0,0]^T$, where f_x and f_l denote the force applied to the cart and the force applied to the cable *l*, respectively. The 3DOC system includes a single pendulum and a moving trolley: *x*, *y* denote the position of the trolley, ϕ, θ are the swing angles, and the position of the cargo is related to the length *l* of the rope. m_x,m_y,m_l are the equivalent masses of the rotating part flows x,y,l, and m is the load mass. The driving forces along the x-direction, the y-direction, and the z-direction are f_x,f_y,f_l, respectively and $\mathbf{U}=[f_x;f_y;f_l;0;0]$ is the force applied to the 3DOC system, with a state vector $\mathbf{q}=[x,y,l,\phi,\theta]^T$.

The Euler–Lagrange approach is followed to derive the equations of motion of industrial cranes [25, 26]. The dynamics of the system, including friction and disturbance, can be written in matrix form as:

$$\mathbf{M}(\mathbf{q})\ddot{\mathbf{q}}+\mathbf{C}(\mathbf{q},\dot{\mathbf{q}})\dot{\mathbf{q}}+\mathbf{G}(\mathbf{q})+\mathbf{F}_b(\mathbf{q},\dot{\mathbf{q}},\ddot{\mathbf{q}})+\mathbf{D}=\mathbf{U} \quad (1)$$

where $\mathbf{M}(\mathbf{q})\in\Re^{5\times5}$ is the mass matrix, $\mathbf{C}(\mathbf{q},\dot{\mathbf{q}})\in\Re^{5\times5}$ is the inertial matrix, $\mathbf{G}(\mathbf{q})\in\Re^{5\times1}$ is the vector gravity, $\mathbf{F}_b(\mathbf{q},\dot{\mathbf{q}},\ddot{\mathbf{q}})\in\Re^{5\times1}$ denotes vector friction, and $\mathbf{D}\in\Re^{5\times1}$ is the external disturbance.

(a)

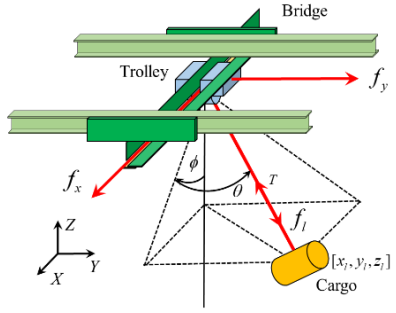

(b)

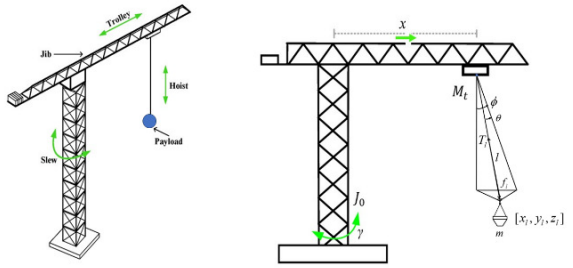

Fig. 1. Industrial crane models: (a) Overhead crane, (b) tower crane.

III. FLATNESS SYSTEM

Formulated upon flat theory principles, the proposed methodology first forms the load motion and then recalculates system states. This two-step approach aims to achieve a dual benefit: reducing computational burden and enhancing real-time control capabilities. Research shows that the tower crane system is a flat system, meaning that the reference signal of the crane $\mathbf{q} = [\gamma, x, l, \phi, \theta]^T$ and the control signal $U_a = [\tau_\gamma, f_x, f_l]^T$ can be derived from the flat output.

The assumption is that the payload is a point mass located at coordinates $[x_l, y_l, z_l]$ and representing the flat output by $\mathbf{y}_0 = [x_l, y_l, z_l]^T$. Therefore, the 3DTC system becomes a flat system. This implies that the following conditions hold satisfyingly:

1. The system's flat output $\mathbf{y}_0$ can be expressed as a function of the state $\mathbf{q}$, the control input $\mathbf{U}_a$, and a finite number of its derivatives: $\mathbf{y}_0 = \mathrm{Y}(\mathbf{q}, \mathbf{U}_a, \dot{\mathbf{U}}_a, ..., \mathbf{U}_a^{(n)})$

2. The desired state $q = [\gamma, x, l, \phi, \theta]^T$ and control input $U_a = [\tau_\gamma, f_x, f_l]^T$ can be expressed entirely in terms of the flat output $\mathbf{y}_0$, and its derivatives by:

$$\mathbf{q} = g_q(\mathbf{y}_0, \dot{\mathbf{y}}_0, \ddot{\mathbf{y}}_0)$$

$$\mathbf{U}_a = g_f(\mathbf{y}_0, \dot{\mathbf{y}}_0, \ddot{\mathbf{y}}_0, \mathbf{y}_0^{(3)}, \mathbf{y}_0^{(4)})$$

Based on the definition of the flat output, the load's position can be determined utilizing the system's states through:

$$\begin{cases} x_l = x\cos(\gamma) + l\sin(\phi)\cos(\theta) \\ y_l = x\sin(\gamma) + l\sin(\theta) \\ z_l = h - l\cos(\phi)\cos(\theta) \end{cases} \quad (2)$$

where h is the height of the crane. Condition 1 is satisfied by (2) which means that $\mathbf{y}_0 = \mathrm{Y}(\mathbf{q}, \mathbf{U}_a, \dot{\mathbf{U}}_a, ..., \mathbf{U}_a^{(n)})$. According to Newton's laws, the crane's motion is described by:

$$\begin{cases} m\ddot{x}_l = -T\cos\theta\sin\phi \\ m\,\ddot{y}_l = T\sin\theta \\ m\,\ddot{z}_l = T\cos\theta\cos\phi - mg \end{cases} \quad (3)$$

where T is the tension in the string. Based on the calculations performed in (3), the swing angles can be determined from the flat output:

$$\begin{cases} \phi = \arctan\left(-\dfrac{\ddot{x}_l}{\ddot{z}_l + g}\right) \\ \theta = \arctan\left(\dfrac{\ddot{y}_l}{\sqrt{\ddot{x}_l^{\,2} + (g + \ddot{z}_l)^2}}\right) \end{cases} \quad (4)$$

By replacing the expression from (4) with the load position (2), an equation for the cart's position and length can be derived:

$$\begin{cases} \gamma = \gamma(x_l, y_l, z_l, \ddot{x}_l, \ddot{y}_l, \ddot{z}_l) \\ x = x(x_l, y_l, z_l, \ddot{x}_l, \ddot{y}_l, \ddot{z}_l) \\ l = (h - z_l)\sqrt{\dfrac{\ddot{x}_l^{\,2}}{(g + \ddot{z}_l)^2} + 1}\sqrt{\dfrac{\ddot{y}_l^2}{\ddot{x}_l^{\,2} + (g + \ddot{z}_l)^2} + 1} \end{cases} \quad (5)$$

Similar to 3DTC, the study also demonstrates that 3DOC is a flat system. Therefore, the state signals and control input U of the 3DOC system is represented as a flat output y_0, with the swing angle of the payload described by (4) and the position of the cart and the cable described by (6):

$$\begin{cases} x = x_l + (h - z_l)\dfrac{\ddot{x}_l}{g + \ddot{z}_l}\dfrac{\sqrt{\dfrac{\ddot{y}_l^{\,2}(\ddot{x}_l^{\,2} + (g + \ddot{z}_l)^2}{\ddot{x}_l^{\,4}} + 1}}{\sqrt{\dfrac{\ddot{y}_l^{\,2}}{\ddot{x}_l^{\,2} + (g + \ddot{z}_l)^2} + 1}} \\ y = y_l - (h - z_l)\dfrac{\ddot{y}_l}{g + \ddot{z}_l} \\ l = (h - z_l)\sqrt{\dfrac{\ddot{x}_l^{\,2}}{(g + \ddot{z}_l)^2} + 1}\sqrt{\dfrac{\ddot{y}_l^2}{(\ddot{x}_l^{\,2} + (g + \ddot{z}_l)^2)} + 1} \end{cases} \quad (6)$$

Equations (4)-(6), exhibit that $\mathbf{q}$ satisfies the equation $\mathbf{q} = g_q(\mathbf{y}_0, \dot{\mathbf{y}}_0, \ddot{\mathbf{y}}_0)$, so $\dot{\mathbf{q}} = g_q(\dot{\mathbf{y}}_0, \ddot{\mathbf{y}}_0, \mathbf{y}_0^{(3)})$ and

$\ddot{\mathbf{q}} = g_q(\ddot{\mathbf{y}}_0, \mathbf{y}_0^{(3)}, \mathbf{y}_0^{(4)})$. Substituting the values of $\mathbf{q}$, $\dot{\mathbf{q}}$, and $\ddot{\mathbf{q}}$ into (1), the forces affecting the industrial crane system can be described by $g_f(\mathbf{y}_0, \dot{\mathbf{y}}_0, \ddot{\mathbf{y}}_0, \mathbf{y}_0^{(3)}, \mathbf{y}_0^{(4)})$.

The desired trajectory ($\mathbf{q}_d$) and control input ($\mathbf{U}_{flat}$) for the crane can be determined based on the position and its derivatives of the payload. This is achieved by calculating $\mathbf{q}_d = g_q\left(\mathbf{y}_{0d}(t), \dot{\mathbf{y}}_{0d}(t), \ddot{\mathbf{y}}_{0d}(t)\right)$ for the desired trajectory and $\mathbf{U}_{flat} = g_f\left(\mathbf{y}_{0d}(t), \dot{\mathbf{y}}_{0d}(t), \ddot{\mathbf{y}}_{0d}(t), \mathbf{y}_{0d}^{(3)}, \mathbf{y}_{0d}^{(4)}\right)$ for the control signal reference. These calculated values will be used as inputs for the following sections.

IV. MODEL PREDICION CONTROL BASE FLATNESS

In the 3DTC system, the controller input $\mathbf{U} = [\tau_\gamma, fx, fy, 0, 0]^T$ is always constrained due to the actuator being powered by a limited power. Therefore, during the controller design process, it is necessary to consider the limitations of the controller's capabilities. To solve this problem, the MPC is employed to control the crane systems. Let $\mathbf{z} = [\mathbf{q}, \dot{\mathbf{q}}]^T$. Then, the system becomes:

$$\dot{\mathbf{z}} = \begin{bmatrix} \dot{\mathbf{q}} \\ \mathbf{M}^{-1}(\mathbf{q})\left(\mathbf{U} - \mathbf{C}(\mathbf{q}, \dot{\mathbf{q}})\dot{\mathbf{q}} - \mathbf{G}(\mathbf{q}) - \mathbf{D}\right) \end{bmatrix} = \mathbf{f}\left(\mathbf{z}, \mathbf{U}\right) \quad (7)$$

In the discrete domain, the system equation becomes:

$$\mathbf{z}(k+1) = \mathbf{f}\left(\mathbf{z}(k), \mathbf{U}(k)\right)$$

The MPC controller implements the initial portion of the finite-horizon optimal solution as the control input for the 3DTC system. A time-invariant prediction horizon defined as $T_p = N_p T_s$, where N_p represents the number of future steps to be predicted and T_s is the discrete sampling time between each prediction step, was considered. Based on this horizon, the cost function was formulated:

$$\begin{aligned} J(k) = &\sum_{j=1}^{N_p} \left\|\hat{\mathbf{e}}(k+j \mid k)\right\|_P^2 \\ &+ \sum_{j=1}^{N_p-1} \left\|\Delta\hat{\mathbf{U}}_1(k+j \mid k)\right\|_Q^2 + \sum_{j=1}^{N_p-1} \left\|\Delta\hat{\mathbf{U}}_2(k+j \mid k)\right\|_R^2 \end{aligned} \quad (8)$$

subject to:

$$\begin{aligned} &\hat{\mathbf{z}}(k+j \mid k) = \mathbf{f}\left(\mathbf{z}(k+j-1 \mid k), \mathbf{U}(k+j-1 \mid k)\right) \\ &(\forall j = 1, 2, \ldots N_p) \\ &\left|\hat{\mathbf{z}}(k+j \mid k)\right| \leqslant \mathbf{z}_{\max} \quad \forall j = 1, 2, \ldots N_p - 1 \\ &\left|\hat{\mathbf{U}}(k+j \mid k)\right| \leqslant \mathbf{U}_{\max} \quad \forall j = 1, 2, \ldots N_p \end{aligned} \quad (9)$$

where $\hat{\mathbf{z}}(k+j \mid k)$, $\hat{\mathbf{U}}(k+j \mid k)$ are the predicted state and the predicted output at sampling $k+j$, given by the current state $\mathbf{z}(k), \mathbf{U}(k)$, $\hat{\mathbf{e}}(k+j \mid k) = \hat{\mathbf{z}}(k+j \mid k) - \mathbf{z}_r(k+j \mid k)$ is the predictive error output and state, $\Delta\hat{\mathbf{U}}_1(k+j \mid k) = \hat{\mathbf{U}}(k+j \mid k) - \hat{\mathbf{U}}_{\text{flat}}(k+j \mid k)$ is the predicted input error between the predicted input and the calculated input from the flatness at time $k+j$, $\Delta\hat{\mathbf{U}}_2(k+j \mid k) = \hat{\mathbf{U}}(k+j \mid k) - \hat{\mathbf{U}}(k+j-1 \mid k)$ is the predicted input error between the predicted inputs at two consecutive times ($k+j-1$ and $k+j$), and, P, Q, and R are positive definite weighted matrices. The controller deployed sample time T_s for solving the loop. At each loop the controller minimizes the cost function $J(k)$ to archive the control signals $\mathbf{U}(k)$. After each cycle, the optimal solution is determined:

$$\boldsymbol{\mu}^*(k) = \operatorname{argmin} J(k)$$

with:

$$\boldsymbol{\mu}\left(k\right) = \left[\hat{\mathbf{U}}(k), \hat{\mathbf{U}}\left(k+1 \mid k\right), \ldots, \hat{\mathbf{U}}\left(k+N_p-1 \mid k\right)\right].$$

The first value $\hat{\mathbf{U}}^*(k)$ of $\boldsymbol{\mu}^*(k)$ is taken as the control signal at period k. This process will be continued in the next computation cycles.

The detailed steps of the closed-loop control are presented in Algorithm 1, while Figure 2 depicts the overall control scheme.

Algorithm 1: Nonlinear Model Predictive Control base Flatness Algorithm

1. Using flatness theory, the reference destination is inputted to determine the solution: $\mathbf{q}_d = g_q\left(\mathbf{y}_{0d}(t), \dot{\mathbf{y}}_{0d}(t), \ddot{\mathbf{y}}_{0d}(t)\right)$ and the reference control signal:

   $$\mathbf{U}_d = g_f\left(\mathbf{y}_{0d}(t), \dot{\mathbf{y}}_{0d}(t), \ddot{\mathbf{y}}_{0d}(t), \mathbf{y}_{0d}^{(3)}, \mathbf{y}_{0d}^{(4)}\right)$$

2. Measure the current state $\mathbf{q}(t_k), \dot{\mathbf{q}}(t_k)$.
3. The current state $\mathbf{q}(t_k)$ and $\dot{\mathbf{q}}(t_k)$, the desired trajectory $\mathbf{q}_d = g_q\left(\mathbf{y}_{0d}(t), \dot{\mathbf{y}}_{0d}(t), \ddot{\mathbf{y}}_{0d}(t)\right)$, and the reference control signal $\mathbf{U}_d = g_f\left(\mathbf{y}_{0d}(t), \dot{\mathbf{y}}_{0d}(t), \ddot{\mathbf{y}}_{0d}(t), \mathbf{y}_{0d}^{(3)}, \mathbf{y}_{0d}^{(4)}\right)$ are applied as inputs to the MPC to find the value of the cost function J that satisfies the accompanying constraints.
4. A solution to the MPC problem is presented in (8), considering the constraints of (9). This process results in a (sub-) optimal solution for the control input $\mathbf{U}(t_k)$.
5. Execute the 3DTC system under the influence of the control signal $\mathbf{U}(t_k)$.
6. After each sampling period T_s, update $t_k = t_k + T_s$ and iterate from step 2.

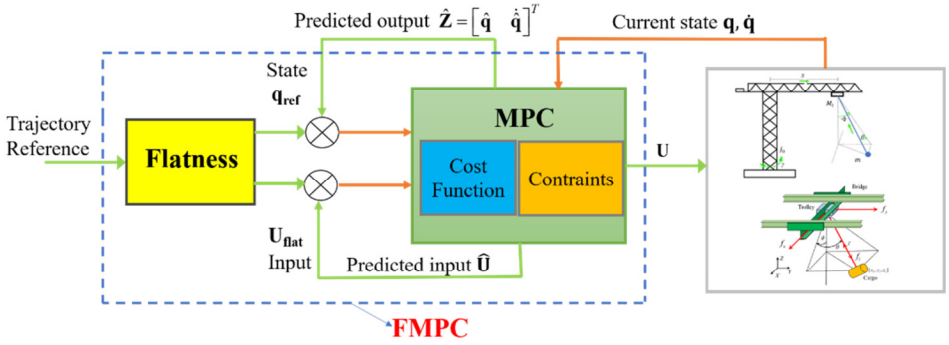

Fig. 2. Closed-loop control system diagram.

V. SIMULATION RESULTS

This section refers to the utilization of the 3DTC and 3DOC crane models with parameter values: $M_t = 3.56$ kg, $m = 2.05$ kg, $J_0 = 6.78$ kgm^2, $b_\gamma = 39$ Nm/s, $b_x = 89$ Nm/s, $b_l = 29$ Nm/s, $g = 9.81$ m/s^2, and $M_x = 12$ kg, $M_y = 5$ kg, $M_l = 2$ kg, $m = 0.85$ kg, $D_x = 20$ Nm/s. $D_y = 30$ Nm/s, and $D_z = 50$ Nm/s. The parameters of the MPC base flatness (FMPC) are as follows: The number of prediction horizon steps is $N_p = 10$, the constraint of the input control force and the swing angles are $U_{\max} = 100$ N, $\Phi_{\max} = 0.1$ rad, and $\theta_{\max} = 0.1$ rad, respectively. The reference trajectories of the 3DTC and 3DOC loads are chosen as:

$$[x_{load}; y_{load}; z_{load}] = [0.3 + 0.02t; 3 + 0.04t; 0.7 + 0.3sin(0.5t)]$$

$$[x_{load}; y_{load}; z_{load}] = [0.1 + 0.01t; 0.3 + 0.03t; 0.3 + 0.5sin(0.01t)]$$

accordingly. The simulation results are verified in the two cases, outlined below.

A. Case 1

In order to determine the best sampling time for the proposed controller, comparison results between 3 different cases of sampling time $T_s = \{0.05$ s; 0.01 s; 0.005 s$\}$ are provided.

In Figure 3, it can be observed that the tracking and antivibration control results of the proposed controller are very good for both model systems. The position coordinates of the loads (flat outputs) in Figure 4 prove the correctness of the selected flat output. These results also disclose that the smaller the sampling time is, the better the tracking and anti-vibration control results are. However, to ensure smooth operations in practice, the T_s value cannot be too small. In this paper, $T_s = 0.005$ s was considered.

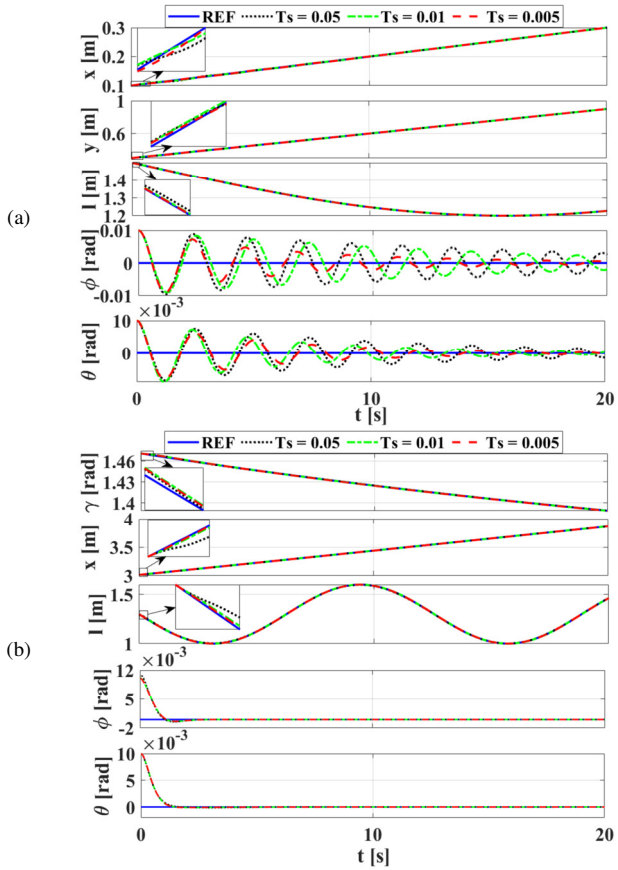

Fig. 3. Output signals of the industrial crane model at three different values of T_s: (a) Gantry crane, (b) of tower crane.

B. Case 2

To show the effectiveness of the FMPC method, this section provides the results of the comparative study between FMPC and MPC at the same sampling time $T_s = 0.005$ s.

Figures 5 and 6 portray the tracking trajectories of the systems designed to be time-varying, which proves that the trajectory of FMPC is better than that of MPC. This is also expressed similarly with load coordinates in Figures 7, 9, and 10. This difference can be clearly noticed in 3DOC models. While the FMPC method gives results close to the reference trajectories of the flat outputs, the MPC results in the

coordinates of load oscillates around the desired values. The vibration angles are also displayed in Figures 5 and 6. Both control methods indicate that the swing angle decreases and converges to zero. Nevertheless, the FMPC method manifests a faster convergence. Figure 8 depicts the control input signals for the system.

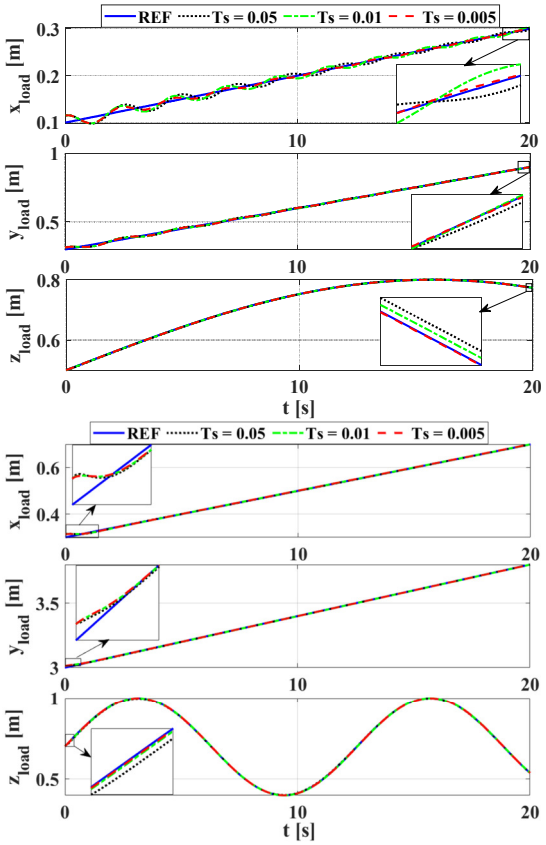

Fig. 4. x_{load}, y_{load}, and z_{load} at three different values of T_s: (a) Gantry crane, (b) of tower crane.

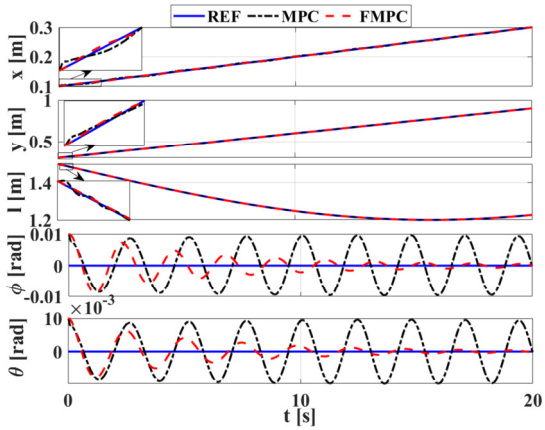

Fig. 5. Output signals of the gantry crane model for MPC and FMPC.

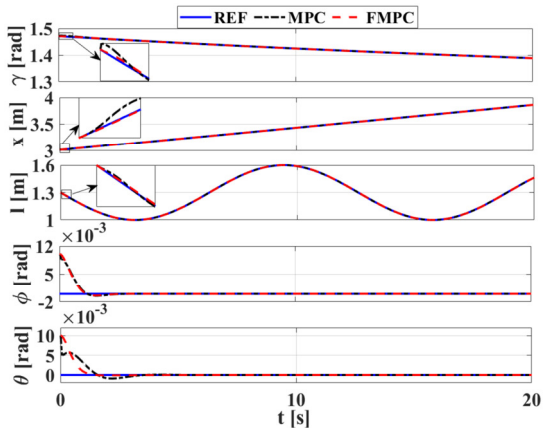

Fig. 6. Output signals of tower crane model for MPC and FMPC.

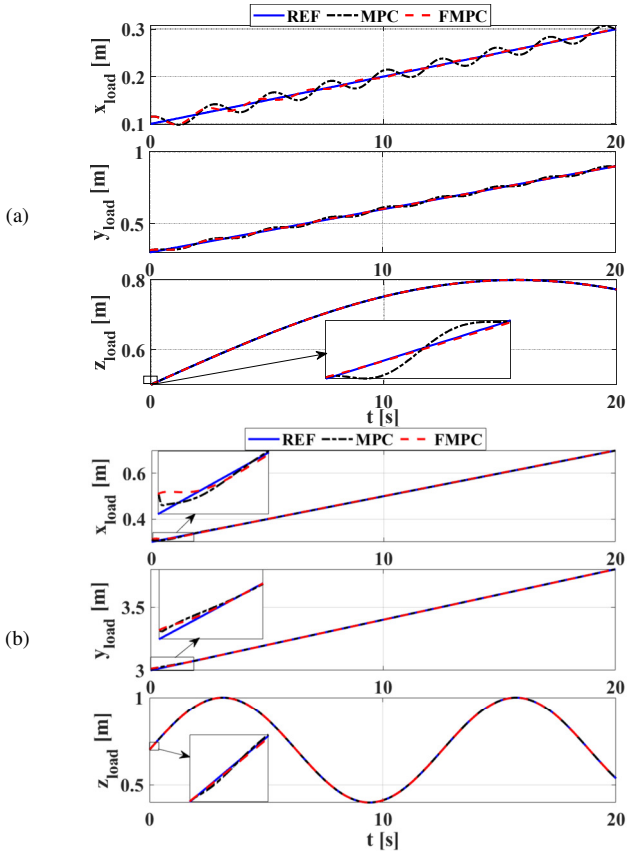

Fig. 7. x_{load}, y_{load}, and z_{load} for MPC and FMPC: (a) Gantry crane, (b) of tower crane.

VI. RESULT ANALYSIS

In order to evaluate the effectiveness of the proposed control, not only the qualitative results, but also the quantitative comparisons of tracking performance and anti-vibration between controllers are implemented. The definitions of the considered performance indexes on the position and the angular errors follow.

(a)

(b)

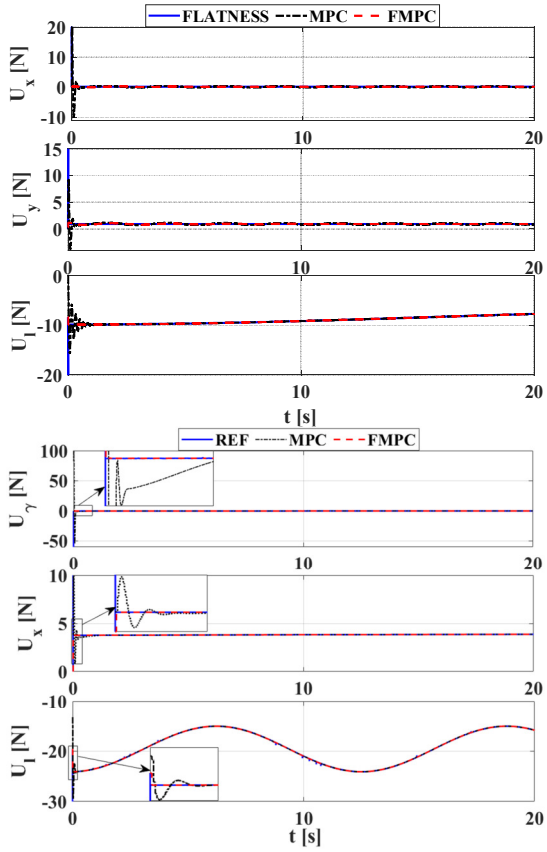

Fig. 8. Input signals of the industrial crane for MPC and FMPC: (a) gantry crane, (b) of tower crane.

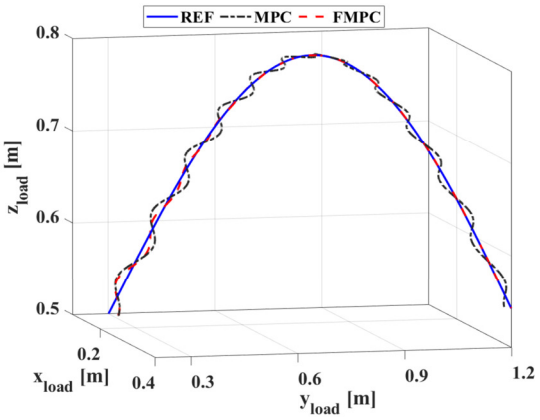

Fig. 9. Load's trajectory of the gantry crane model for MPC and FMPC.

Integral Squared Errors (ISE) of two types are denoted:

$$ISE_p = \int_0^t \sum_i e_i^2(t)dt$$

$$ISE_a = \int_0^t \sum_j e_j^2(t)dt$$

Two types of Integral Time-multiplied Absolute Errors are determined:

$$ITAE_p = \int_0^t t \sum_i |e_i(t)|\, dt$$

$$ITAE_a = \int_0^t t \sum_j |e_j(t)|\, dt$$

where $i = x, y, l_1$ and $j = \phi, \theta$ for the gantry crane or $i = x, y$ and $j = \phi, \theta, \gamma$ for the tower crane, with t denoting the simulation time. Since the ISE index penalizes a larger error more than a smaller one, it can be observed that the designed control law with a lower ISE value provides fast convergence. The ITAE index is more focused on the steady-state error than the initial response. It should be noted that a lower value of these indices indicates a better control result.

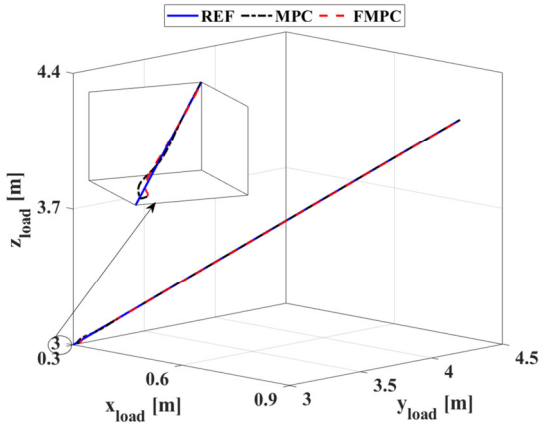

Fig. 10. Load's trajectory of the tower crane model for MPC and FMPC.

In Table I, we can see that the proposed control has the lowest errors compared to other methods. This proves that the flatness-based model predictive control is superior to its predecessors.

TABLE I. EVALUATION INDEX OF CONTROLLERS

Errors	States	FMPC 0.05 s	FMPC 0.01 s	FMPC 0.005 s	MPC
ISE 3DOC	x, y, l_1	0.0075	0.0076	0.0040	0.0945
	ϕ, θ	0.273	0.1258	0.2369	0.6273
ITAE 3DOC	x, y, l_1	51.86	42.298	43.7664	48.37
	ϕ, θ	323.88	161.883	339.406	125.12
ISE 3DTC	x, y	0.0314	0.0063	0.00178	0.0028
	γ, ϕ, θ	0.0690	0.0290	0.0346	0.0378
ITAE 3DTC	x, y	102.98	85.198	46.9923	49.683
	γ, ϕ, θ	7.2059	12.196	18.3313	24.847

VII. CONCLUSION

This research presents an MPC based on flatness for the industrial crane. Thanks to the flatness theory, the reference trajectory of the state variables and input signals is designed based on the flat output of the payload. Besides, through the flat output, the calculation cost and the complication of the proposed control strategy are reduced. The MPC satisfies the limitations of the actuators due to its ability to restrict the state and input signals in authorized spaces. This controller also certifies the state trajectory converging to the desired trajectory. The effectiveness of the proposed controller was demonstrated through simulation results. All system state and input signals are restricted and closely follow the reference trajectory designing from the flat output of the payload, while the swing

angles are quite small and converge to zero. Finally, comparison results with the traditional MPC proved the effectiveness and feasibility of the flatness-based MPC.

ACKNOWLEDGEMENT

This research is funded by Hanoi University of Industry (Haui) under project code10-2023-RD/HĐ-ĐHCN.

REFERENCES

[1] D. Antic, Z. Jovanovic, S. Peric, S. Nikolic, M. Milojkovic, and M. Milosevic, "Anti-Swing Fuzzy Controller Applied in a 3D Crane System," *Engineering, Technology & Applied Science Research*, vol. 2, no. 2, pp. 196–200, Apr. 2012, https://doi.org/10.48084/etasr.146.

[2] B. Spruogis, A. Jakstas, V. Gican, V. Turla, and V. Moksin, "Further Research on an Anti-Swing Control System for Overhead Cranes," *Engineering, Technology & Applied Science Research*, vol. 8, no. 1, pp. 2598–2603, Feb. 2018, https://doi.org/10.48084/etasr.1774.

[3] M. D. Duong, Q. T. Dao, and T. H. Do, "Settling Time Optimization of a Critically Damped System with Input Shaping for Vibration Suppression Control," *Engineering, Technology & Applied Science Research*, vol. 12, no. 5, pp. 9388–9394, Oct. 2022, https://doi.org/10.48084/etasr.5242.

[4] H. Ouyang, Z. Tian, L. Yu, and G. Zhang, "Motion planning approach for payload swing reduction in tower cranes with double-pendulum effect," *Journal of the Franklin Institute*, vol. 357, no. 13, pp. 8299–8320, Sep. 2020, https://doi.org/10.1016/j.jfranklin.2020.02.001.

[5] Z. Tian, L. Yu, H. Ouyang, and G. Zhang, "Swing suppression control in tower cranes with time-varying rope length using real-time modified trajectory planning," *Automation in Construction*, vol. 132, Dec. 2021, Art. no. 103954, https://doi.org/10.1016/j.autcon.2021.103954.

[6] Q. Wu, X. Wang, L. Hua, and M. Xia, "Improved time optimal anti-swing control system based on low-pass filter for double pendulum crane system with distributed mass beam," *Mechanical Systems and Signal Processing*, vol. 151, Apr. 2021, Art. no. 107444, https://doi.org/10.1016/j.ymssp.2020.107444.

[7] T. Ho, K. Suzuki, M. Tsume, R. Tasaki, T. Miyoshi, and K. Terashima, "A switched optimal control approach to reduce transferring time, energy consumption, and residual vibration of payload's skew rotation in crane systems," *Control Engineering Practice*, vol. 84, pp. 247–260, Mar. 2019, https://doi.org/10.1016/j.conengprac.2018.11.018.

[8] G. Li, X. Ma, Z. Li, and Y. Li, "Time-Polynomial-Based Optimal Trajectory Planning for Double-Pendulum Tower Crane With Full-State Constraints and Obstacle Avoidance," *IEEE/ASME Transactions on Mechatronics*, vol. 28, no. 2, pp. 919–932, Apr. 2023, https://doi.org/10.1109/TMECH.2022.3210536.

[9] Z. Liu, T. Yang, N. Sun, and Y. Fang, "An Antiswing Trajectory Planning Method With State Constraints for 4-DOF Tower Cranes: Design and Experiments," *IEEE Access*, vol. 7, pp. 62142–62151, 2019, https://doi.org/10.1109/ACCESS.2019.2915999.

[10] M. Burkhardt, A. Gienger, and O. Sawodny, "Optimization-Based Multipoint Trajectory Planning Along Straight Lines for Tower Cranes," *IEEE Transactions on Control Systems Technology*, vol. 32, no. 1, pp. 290–297, Jan. 2024, https://doi.org/10.1109/TCST.2023.3308762.

[11] Z. Yu and W. Niu, "Flatness-Based Backstepping Antisway Control of Underactuated Crane Systems under Wind Disturbance," *Electronics*, vol. 12, no. 1, Jan. 2023, Art. no. 244, https://doi.org/10.3390/electronics12010244.

[12] B. Kolar, H. Rams, and K. Schlacher, "Time-optimal flatness based control of a gantry crane," *Control Engineering Practice*, vol. 60, pp. 18–27, Mar. 2017, https://doi.org/10.1016/j.conengprac.2016.11.008.

[13] J. Diwold, B. Kolar, and M. Schöberl, "Discrete-time flatness-based control of a gantry crane," *Control Engineering Practice*, vol. 119, Feb. 2022, Art. no. 104980, https://doi.org/10.1016/j.conengprac.2021.104980.

[14] M. Zhang, X. Ma, X. Rong, X. Tian, and Y. Li, "Adaptive tracking control for double-pendulum overhead cranes subject to tracking error limitation, parametric uncertainties and external disturbances," *Mechanical Systems and Signal Processing*, vol. 76–77, pp. 15–32, Aug. 2016, https://doi.org/10.1016/j.ymssp.2016.02.013.

[15] J. Schatz and R. J. Caverly, "Payload trajectory tracking of a 5-DOF tower crane with a varying-length hoist cable: A passivity-based adaptive control approach," *Mechatronics*, vol. 94, Oct. 2023, Art. no. 103027, https://doi.org/10.1016/j.mechatronics.2023.103027.

[16] X. Yao, H. Chen, Y. Liu, and Y. Dong, "Tracking approach of double pendulum cranes with variable rope lengths using sliding mode technique," *ISA Transactions*, vol. 136, pp. 152–161, May 2023, https://doi.org/10.1016/j.isatra.2022.11.019.

[17] T.-S. Wu, M. Karkoub, W.-S. Yu, C.-T. Chen, M.-G. Her, and K.-W. Wu, "Anti-sway tracking control of tower cranes with delayed uncertainty using a robust adaptive fuzzy control," *Fuzzy Sets and Systems*, vol. 290, pp. 118–137, May 2016, https://doi.org/10.1016/j.fss.2015.01.010.

[18] Z. Sun and H. Ouyang, "Adaptive fuzzy tracking control for vibration suppression of tower crane with distributed payload mass," *Automation in Construction*, vol. 142, Oct. 2022, Art. no. 104521, https://doi.org/10.1016/j.autcon.2022.104521.

[19] X. Miao, H. Zhu, S. Li, X. Xu, H. Ouyang, and H. Xi, "Adaptive-back-stepping-based controller design for double-pendulum rotary cranes," *ISA Transactions*, vol. 136, pp. 676–686, May 2023, https://doi.org/10.1016/j.isatra.2022.11.011.

[20] W. Zhang, H. Chen, X. Yao, and D. Li, "Adaptive tracking of double pendulum crane with payload hoisting/lowering," *Automation in Construction*, vol. 141, Sep. 2022, Art. no. 104368, https://doi.org/10.1016/j.autcon.2022.104368.

[21] S. M. F. ur Rehman *et al.*, "Adaptive input shaper for payload swing control of a 5-DOF tower crane with parameter uncertainties and obstacle avoidance," *Automation in Construction*, vol. 154, Oct. 2023, Art. no. 104963, https://doi.org/10.1016/j.autcon.2023.104963.

[22] Z. Wu, X. Xia, and B. Zhu, "Model predictive control for improving operational efficiency of overhead cranes," *Nonlinear Dynamics*, vol. 79, no. 4, pp. 2639–2657, Mar. 2015, https://doi.org/10.1007/s11071-014-1837-8.

[23] T. Bariša, M. Bartulović, G. Žužić, Š. Ileš, J. Matuško, and F. Kolonić, "Nonlinear predictive control of a tower crane using reference shaping approach," in *2014 16th International Power Electronics and Motion Control Conference and Exposition*, Sep. 2014, pp. 872–876, https://doi.org/10.1109/EPEPEMC.2014.6980608.

[24] Š. Ileš, J. Matuško, and F. Kolonić, "Sequential distributed predictive control of a 3D tower crane," *Control Engineering Practice*, vol. 79, pp. 22–35, Oct. 2018, https://doi.org/10.1016/j.conengprac.2018.07.001.

[25] M. Egretzberger, K. Graichen, and A. Kugi, "Flatness-Based MPC and Global Path Planning Towards Cognition-Supported Pick-and-Place Tasks of Tower Cranes," in *Advanced Dynamics and Model-Based Control of Structures and Machines*, H. Irschik, M. Krommer, and A. K. Belyaev, Eds. Vienna, Austria: Springer, 2012, pp. 63–71.

[26] E. M. Abdel-Rahman, A. H. Nayfeh, and Z. N. Masoud, "Dynamics and Control of Cranes: A Review," *Journal of Vibration and Control*, vol. 9, no. 7, pp. 863–908, Jul. 2003, https://doi.org/10.1177/1077546303009007007.